

# Efficient Gridless DoA Estimation Method of Non-uniform Linear Arrays with Applications in Automotive Radars

Silin Gao, Zhe Zhang, *Member, IEEE*, Muhan Wang, Yan Zhang, Jie Zhao, Bingchen Zhang, Yue Wang, *Senior Member, IEEE* and Yirong Wu

**Abstract**—This paper focuses on the gridless direction-of-arrival (DoA) estimation for data acquired by non-uniform linear arrays (NLAs) in automotive applications. Atomic norm minimization (ANM) is a promising gridless sparse recovery algorithm under the Toeplitz model and solved by convex relaxation, thus it is only applicable to uniform linear arrays (ULAs) with array manifolds having a Vandermonde structure. In automotive applications, it is essential to apply the gridless DoA estimation to NLAs with arbitrary geometry with efficiency. In this paper, a fast ANM-based gridless DoA estimation algorithm for NLAs is proposed, which employs the array manifold separation technique and the accelerated proximal gradient (APG) technique, making it applicable to NLAs without losing of efficiency. Simulation and measurement experiments on automotive multiple-input multiple-output (MIMO) radars demonstrate the superiority of the proposed method.

**Index Terms**—Atomic norm minimization, gridless DoA estimation, non-uniform linear array, automotive radars.

## I. INTRODUCTION

**D**IRECTION-of-arrival (DoA) estimation is an important area in array signal processing, which holds paramount importance in a multitude of applications, including but not limited to radar, sonar, wireless communication, and microphone arrays. DoA estimation is of critical importance in automotive radar systems, which are used in advanced driver assistance systems (ADAS) and autonomous vehicles for safety and navigation purposes. Automotive radar systems rely on DoA estimation to accurately detect and locate objects such as other vehicles, pedestrians, and obstacles on the road.

Plenty of DOA algorithms have been proposed in the last decades. Classical beamforming methods, such as Bartlett algorithm and minimum variance distortionless response (MVDR) algorithm [1] can effectively perform filtering in the

spatial domain thus enabling DoA estimation. However, the theoretical resolution depends mainly on the array aperture and strictly limited by the Rayleigh resolution. Subspace algorithms, such as the multiple signal classification (MUSIC) [2], [3] algorithm and the estimation of signal parameters via rotational invariance techniques (ESPRIT) [4]–[7] algorithm has the super-resolution ability. However, it needs multiple snapshots (multiple measurement vector or MMV) of data and a high signal-to-noise ratio (SNR), as well as incoherent signal sources.

In the recent decades, sparse signal processing based techniques such as compressed sensing (CS) techniques [8]–[10] has been introduced into DoA estimation by exploiting the sparsity structure of the signal. [11], [12] solves the DoA estimation problem by leveraging the spatial domain discretization and the  $\ell_1$  norm regularization model, making it applicable to single snapshot (SMV) and/or coherent scenarios. However, the spatial domain discretization suffers the grid mismatching problem [13]. Tackling this issue, the straightforward approach is to increase the grid density, such as the iterative grid refinement (IGR) technique [14]. However, using a dense set of grids will violate the restricted isometry property (RIP) [15] thus resulting the sparse reconstruction impossible.

Aiming at the gridding effect, the off-grid DOA estimation model is first proposed in [16] to parameterize the off-grid error as a model perturbation. References [17]–[20] improve the off-grid signal model and solve it via sparse Bayesian learning (SBL), but suffering from complicated parameter tuning and high computational load.

Atomic norm minimization (ANM) is the cutting-edge development of sparse signal processing [21]. Different from the perturbation based methods, ANM directly constructed a gridless sparse model from scratch. Retaining the benefit of gridless output and super-resolution ability, ANM does not require incoherent signal sources and works smoothly with single snapshot. However, currently ANM is mainly solved via semi-positive definite programming (SDP) and relies on the Vandermonde structure of atoms. For array signal processing, only data acquired by uniform linear arrays (ULAs) can be processed by the ANM algorithm. [22]–[27] generalize ANM to the sparse arrays or incomplete data. However, in practical situations, it is often not possible to select the array geometry from some narrow categories. Therefore, it is of great significance to study the ANM algorithm that applicable to arbitrary non-uniform linear arrays (NLAs).

Corresponding author: Zhe Zhang (zhangzhe01@aircas.ac.cn)

S. Gao, Z. Zhang, M. Wang, Y. Zhang, B. Zhang and Y. Wu are with Aerospace Information Research Institute, Chinese Academy of Sciences, Beijing, China.

S. Gao, M. Wang, Y. Zhang, B. Zhang and Y. Wu are also with Key Laboratory of Technology in Geo-spatial Information Processing and Application System, Chinese Academy of Sciences, Beijing, China, and School of Electronic, Electrical and Communication Engineering, University of Chinese Academy of Sciences, Beijing, China.

Z. Zhang and M. Wang are also with Suzhou Key Laboratory of Microwave Imaging, Processing and Application Technology, and Suzhou Aerospace Information Research Institute, Suzhou, Jiangsu, China.

Jie Zhao is with the Beijing Autoroad Tech Co., Ltd.

Yue Wang is with Electrical and Computer Engineering Department, George Mason University, Fairfax, VA, USA.

In this paper, we study the gridless DoA estimation problem for off-grid targets in automotive radar applications. We propose a fast gridless DoA estimation algorithm for NLAs based on ANM, namely FNLANM algorithm. The proposed algorithm uses the array manifold separation technique [28]–[30] to transform the physical (non-uniform) array into a virtual uniform array. The original array manifold is given as the product of a sampling matrix and a (uniform) Vandermonde vector, thus expanding the capability of ANM algorithm to arbitrary linear arrays. This optimization problem can also be solved via SDP, but the computational complexity would be impracticable for large virtual arrays. Inspired by [31], we introduce the accelerated proximal gradient (APG) technique into the proposed algorithm to replace the SDP, reducing the computational complexity from  $\mathcal{O}(N_v^{3.5})$  to  $\mathcal{O}(N_v^2)$ , where  $N_v$  is the number of virtual array elements.

The rest of this paper is organized as follows. Section II describes the background of automotive radars, establishes the signal model, and introduces the grid-based CS algorithms for DoA estimation. The concept of ANM and gridless DoA estimation algorithm for ULAs are given in Section III. The proposed FNLANM gridless DoA estimation algorithm is also introduced in this section. Numerical analysis are discussed in Section IV, followed by the measured data results shown in Section V. Finally, the conclusions are given in Section VI.

Throughout this paper, vectors are denoted by lowercase bold characters (e.g.  $\mathbf{v}$ ) and matrices by uppercase bold characters (e.g.  $\mathbf{M}$ ).  $(\cdot)^T$  is the transpose operator and  $(\cdot)^H$  is the Hermitian transpose operator.

## II. BACKGROUNDS

This section provides some preliminary backgrounds of this paper, including automotive radar model, NLA signal model, and canonical compressed sensing based DoA estimation methods.

### A. Automotive radars

Automotive radars transmit electromagnetic wave and receive echoes to detect nearby objects. To obtain both the range and velocity of targets, frequency modulated continuous wave (FMCW) is commonly used as the transmitting waveform in automotive radars, which can provide good detection performance in complex traffic situations with multiple targets [32].

Commercial FMCW radars, which usually work at 77 GHz mmWave band, can easily achieve high resolution in range and velocity. To achieve angular resolving ability, automotive radars have evolved from using ULAs to multiple-input multiple-output (MIMO) arrays. ULAs that satisfying the Nyquist sampling theorem are the most commonly employed arrays. For ULAs, improving the angular resolution requires enlarged array aperture as well as huge amount of elements to, which implies increased hardware cost and computational complexity [33]. In recent years, MIMO technology has become increasingly popular in the design of automotive radars. This is primarily due to its ability to enhance radar performance and boost angular resolution, thereby improving the overall capabilities [34], [35]. Constructing virtual arrays

with larger apertures is the technique employed in MIMO radars to achieve higher angular resolution, and the virtual arrays are usually NLAs.

NLAs offer many advantages over ULAs with the same number of elements. The non-uniform spacing between elements provides more information about about the received signal, which can improve the angular resolution. NLAs can have reduced sidelobe levels compared to ULAs, which can improve the ability to detect weak targets in the presence of noise and interference. NLAs offers more design flexibility and lower cost of second design and implementation than ULAs with the same performance.

Overall, the use of NLAs in automotive radar systems offers a number of benefits that can significantly enhance the overall performance. Therefore, it is necessary for us to study advanced signal processing methods applicable to NLAs, especially the DoA estimation algorithms.

### B. Signal model

It is assumed that the linear array consists of  $N$  array elements. With  $E_0$  as the reference array element, the positions of each array elements are written as  $\mathbf{r} = [0 \ r_1 \ \dots \ r_{N-1}]^T$ . Note that we do not assume the  $\mathbf{r}$  to be evenly distributed, i.e. it can be an arbitrary configured linear array. In general, we assume that the array elements are isotropic, that there is no error in spatial location, no coupling among the array elements, and no extra error in the received response. The sources are assumed to be far-field, so the received signal is approximated as a plane wave when it arrives at the array. The subsequent sections are based on those assumptions.

Fig. 1 shows a schematic diagram of a linear array receiving signals with DoA angle  $\theta$ . The array manifold of this linear array can be expressed as:

$$\mathbf{a}(\theta) = \left[ 1 \quad e^{j2\pi \frac{r_1}{\lambda} \cos \theta} \quad \dots \quad e^{j2\pi \frac{r_{N-1}}{\lambda} \cos \theta} \right]^T. \quad (1)$$

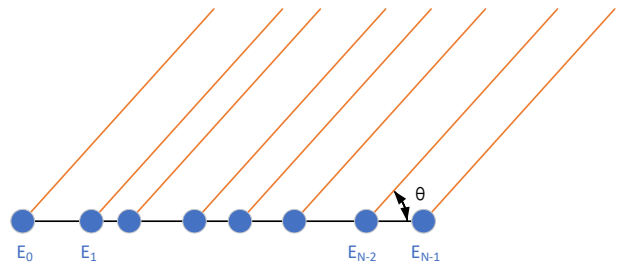


Fig. 1: Linear array schematic.

For a noisy scenario with  $K$  targets located at  $K$  different directions, the signal  $\mathbf{x}$  received by the array can be written as:

$$\mathbf{x} = \sum_{k=1}^K c_k \mathbf{a}(\theta_k) + \mathbf{n}, \quad (2)$$

where

- $c_k$  is the reflectivity of the  $k$ -th target;
- $\theta_k$  is the direction of the  $k$ -th target;
- $\mathbf{n}$  is the additive Gaussian white noise.

We need to recover  $\{(c_k, \theta_k)\}$  from the observed  $\mathbf{x}$ . There are a number of well-established algorithms available to accurately locate targets in linear arrays. Currently, the most widely used method for single snapshot NLA DoA estimation is compressed sensing, or CS based methods.

### C. DoA via CS method

CS is a grid-based method, which discretize  $\theta \in (0, \pi)$  into  $M$  virtual grids and define a basis set of steering vectors  $\mathbf{a}(\theta)$  as  $\mathcal{A}_M = \{\mathbf{a}(\theta) : \theta \in (0, \frac{1}{M}\pi, \dots, \frac{M-1}{M}\pi)\}$ . Therefore, the sparsity of the scenario can be defined as the  $\ell_0$  norm (and relaxed to the  $\ell_1$  norm) of  $\mathbf{x}$  over the basis  $\mathcal{A}_M$  as:

$$\|\mathbf{x}\|_{\mathcal{A}_M,0} = \inf \left\{ K : \sum_{k=1}^K \hat{c}_k \mathbf{a}(\hat{\theta}_k) = \mathbf{x}, \mathbf{a}(\hat{\theta}_k) \in \mathcal{A}_M \right\}, \quad (3)$$

$$\|\mathbf{x}\|_{\mathcal{A}_M,1} = \inf \left\{ \sum_{k=1}^K |\hat{c}_k| : \sum_{k=1}^K \hat{c}_k \mathbf{a}(\hat{\theta}_k) = \mathbf{x}, \mathbf{a}(\hat{\theta}_k) \in \mathcal{A}_M \right\} \quad (4)$$

In the compressed sensing framework, it is proved that we can recover  $\{\theta_k\}$  and  $\{c_k\}$  via relaxed convex  $\ell_1$  norm minimization under some conditions [15]. Therefore, the DoA information of targets can be obtained by solving the optimization problem based on  $\ell_1$  norm minimization as follows:

$$\min_{\mathbf{c}} \frac{1}{2} \|\mathbf{x} - \mathbf{A}\mathbf{c}\|_2^2 + \gamma \|\mathbf{x}\|_{\mathcal{A}_M,1}, \quad (5)$$

where

- $\mathbf{A}$  is the  $N \times M$  observation matrix with  $[\mathbf{A}]_{n,m} = e^{j2\pi \frac{r_{n-1}}{\lambda} \cos \frac{m-1}{M}\pi}$ ;
- $\mathbf{c}$  is the discrete reflectivity vector in the grids;
- $\gamma$  is a factor related to the noise level.

This  $\ell_1$  norm minimization problem (5) can be solved by the iterative shrinkage thresholding algorithm (ISTA), a classic grid-based CS algorithm. Other mature CS recovery algorithms such as orthogonal matching pursuit (OMP) and compressive sampling matching pursuit (CoSaMP) can also be applied to this inversion problem.

## III. PROPOSED METHOD

In this section, we introduce the concept of atomic norm and present an ANM-based DoA estimation algorithm for ULAs. Then we will extend it to NLAs by introducing the array manifold separation technique and the accelerated proximal gradient technique. Finally, a fast gridless DoA estimation algorithm based on ANM for NLAs is proposed.

### A. DoA via ANM for ULAs

The grid-based CS algorithms assume that targets are located on discrete grids, which is an assumption that is inconsistent with the fact that the targets are usually off the grids, i.e.,  $\mathbf{a}(\theta_k) \notin \mathcal{A}_M$ , resulting in the grid mismatch issue. ANM addresses this issue by manipulating  $M \rightarrow \infty$ ,

leveraging  $\mathcal{A} = \{\mathbf{a}(\theta) : \theta \in (0, \pi)\}$ . Then, we can define the gridless version of Eq. (3) and Eq. (4) as

$$\|\mathbf{x}\|_{\mathcal{A},0} = \inf \left\{ K : \sum_{k=1}^K \hat{c}_k \mathbf{a}(\hat{\theta}_k) = \mathbf{x}, \mathbf{a}(\hat{\theta}_k) \in \mathcal{A} \right\}, \quad (6)$$

$$\begin{aligned} \|\mathbf{x}\|_{\mathcal{A}} &= \|\mathbf{x}\|_{\mathcal{A},1} \\ &= \inf \left\{ \sum_{k=1}^K |\hat{c}_k| : \sum_{k=1}^K \hat{c}_k \mathbf{a}(\hat{\theta}_k) = \mathbf{x}, \mathbf{a}(\hat{\theta}_k) \in \mathcal{A} \right\}. \end{aligned} \quad (7)$$

Theoretically,  $\{\theta_k\}$  can be obtained by solving following optimization problem:

$$\min \|\mathbf{x}\|_{\mathcal{A}}. \quad (8)$$

However, (8) is an infinite programming, which cannot be easily solved via mature convex optimization methods. [21] has proved that when the atoms are in the form of Vandermonde vectors (i.e. it is a ULA with evenly distributed array elements), it can be solved via the following semi-positive definite programming:

$$\begin{aligned} \min_{\hat{\mathbf{x}}, v, \mathbf{T}(\mathbf{u})} \quad & \tau(v + \frac{1}{N} \text{trace}(\mathbf{T}(\mathbf{u}))) + \|\hat{\mathbf{x}} - \mathbf{x}\|_2^2 \\ \text{s.t.} \quad & \begin{pmatrix} v & \hat{\mathbf{x}}^H \\ \hat{\mathbf{x}} & \mathbf{T}(\mathbf{u}) \end{pmatrix} \succeq 0; \end{aligned} \quad (9)$$

where

- $\mathbf{T}(\mathbf{u})$  is a Toeplitz matrix determined by its first row  $\mathbf{u}$ ;
- $\tau$  is a factor related to the noise level.

Eq. (9) is a standard SDP that can be solved via popular convex optimization solvers. Angles  $\{\theta_k\}$  are embedded in  $\mathbf{T}(\mathbf{u})$  and can be revealed via Vandermonde decomposition, and  $\{c_k\}$  can be determined subsequently without difficulty. The algorithm flow for gridless DoA estimation on ULAs by ANM is given in Alg. 1.

---

### Algorithm 1: DoA via ANM for ULAs

---

**Input:**  $\mathbf{x}, \tau, K$ .

**Output:**  $\{(\hat{c}_k, \hat{\theta}_k)\}$ .

1. Solve the SDP problem Eq. (9);
2. Performed eigenvalue decomposition on  $\mathbf{T}(\mathbf{u})$ ;
3. Determine the noise subspace  $\mathbf{U}_N$  based on the number of targets  $K$ ;
4. Define  $\mathbf{p}(z) = [1 \ z \ \dots \ z^{N-1}]^T$ ,  $f(z) = \mathbf{p}^H(z) \mathbf{U}_N \mathbf{U}_N^H \mathbf{p}(z)$  and find the roots of the polynomial  $f(z)$ ;
5. Find the  $K$  roots  $\{z_k\}$  closest to the unit circle;
6. Calculate  $\{\hat{\theta}_k\}$  based on

$$\cos \hat{\theta}_k = \frac{\lambda}{2\pi d} \text{angle}(z_k),$$

where  $\text{angle}(z_k)$  returns the phase angle of  $z_k$  in the interval  $[-\pi, \pi]$ ;

7. The reflectivity  $\{\hat{c}_k\}$  can be calculated by the least squares method.
-

### B. DoA via Fast ANM for NLAs (FNLANM)

ULAs with Vandermonde array manifold are the most well-studied array configuration. However, in practice, physical constraints such as limited space and mounting restrictions often make it challenging to employ ULAs. As mentioned earlier, NLAs offer improved angular resolution and reduced sidelobe levels with fewer elements. NLAs have provided a more practical and effective solution for many practical applications due to their superior performance. To take full advantage of gridless estimation, it is essential to extend the ANM-based DoA estimation approaches to NLAs.

1) *Manifold separation*: Inspired by the array interpolation technique, [36] proposed the concept of the manifold separation technique. Using this method, the array manifold of a NLA can be decomposed into the product of a sampling matrix and a canonical Vandermonde manifold matrix. The sampling matrix describes the array itself and the Vandermonde matrix can be treated as the array manifold of a ULA, which can be used for DoA estimation.

The signal received by the  $n$ -th array element can be rewritten as  $[\mathbf{a}(\theta)]_n$  as:

$$[\mathbf{a}(\theta)]_n = e^{\frac{1}{2}(2\pi\frac{r_{n-1}}{\lambda})(je^{j\theta} - \frac{1}{je^{j\theta}})}. \quad (10)$$

By definition, the coefficients of the Laurent expansion of  $e^{\frac{1}{2}z(t-\frac{1}{t})}$  are the Bessel functions of integer order  $\{J_i(z)\}$ :

$$e^{\frac{1}{2}z(t-\frac{1}{t})} = \sum_{i=-\infty}^{\infty} t^i J_i(z), \quad (11)$$

where  $J_{-i}(z) = (-1)^i J_i(z)$ .

Performing a Laurent expansion of  $[a(\theta)]_n$  according to Eq. (11), we can express (10) as [28], [36], [37]:

$$[\mathbf{a}(\theta)]_n = \sum_{i=-\infty}^{\infty} j^i J_i(2\pi\frac{r_{n-1}}{\lambda}) e^{j\theta i}. \quad (12)$$

One characteristic of the Bessel function is that it decays quickly with  $|i|$ . When  $|i| > \frac{2\pi}{\lambda} r_n$ , it can be shown that  $J_i(2\pi\frac{r_n}{\lambda})$  is very small and we can simply truncate the infinite series by ignoring the higher order terms. Note that the truncated order  $I$  should satisfy the following condition:

$$I > \frac{2\pi}{\lambda} D, \quad (13)$$

where  $D = \max\{r_n\}$  [36].

Then the array manifold can be written as:

$$[\mathbf{a}(\theta)]_n \approx \sum_{i=-I}^I j^i J_i(2\pi\frac{r_{n-1}}{\lambda}) e^{j\theta i} = \mathbf{g}_{n-1}^T \mathbf{v}(\theta_k), \quad (14)$$

$$\text{where } \mathbf{g}_{n-1} = \begin{bmatrix} j^{-I} J_{-I}(2\pi\frac{r_{n-1}}{\lambda}) \\ \vdots \\ J_0(2\pi\frac{r_{n-1}}{\lambda}) \\ \vdots \\ j^I J_I(2\pi\frac{r_{n-1}}{\lambda}) \end{bmatrix}, \quad \mathbf{v}(\theta) = \begin{bmatrix} e^{j\theta(-I)} \\ \vdots \\ 1 \\ \vdots \\ e^{j\theta(I)} \end{bmatrix}.$$

Organizing  $\mathbf{a}(\theta)$  into matrix form according to Eq. (14), we obtain the following result of the array manifold separation as [38]:

$$\mathbf{a}(\theta) = \begin{bmatrix} \mathbf{g}_0^T \\ \mathbf{g}_1^T \\ \vdots \\ \mathbf{g}_{N-1}^T \end{bmatrix} \mathbf{v}(\theta) = \mathbf{G} \mathbf{v}(\theta), \quad (15)$$

where  $\mathbf{G}$  is the  $N \times (2I+1)$  sampling matrix which can be calculated from the real location of array elements or measured by effective aperture distribution function (EADF). Eq. (15) turns the array manifold of a NLA into Vandermonde with length  $2I+1$ , which eventually can be treated as the array manifold of a virtual ULA.

For noisy scenario with  $K$  targets located at  $K$  different directions, the signal  $\mathbf{x}$  received by the array can be written as:

$$\begin{aligned} \mathbf{x} &= \sum_{k=1}^K c_k \mathbf{a}(\theta_k) + \mathbf{n} \\ &= \sum_{k=1}^K c_k \mathbf{G} \mathbf{v}(\theta_k) + \mathbf{n} \\ &= \mathbf{G} \sum_{k=1}^K c_k \mathbf{v}(\theta_k) + \mathbf{n}. \end{aligned} \quad (16)$$

Denote that  $\mathbf{d} = \sum_{k=1}^K c_k \mathbf{v}(\theta_k)$ , then  $\mathbf{d}$  is the signal received by the virtual ULA and is the weighted sum of a series of Vandermonde vectors. As already mentioned in the previous section, for vectors of the form as  $\mathbf{d}$ , we can transform the atomic norm minimization problem into the following SDP:

$$\begin{aligned} \min_{\mathbf{d}, v, \mathbf{T}(\mathbf{u})} \quad & \tau(v + \frac{1}{N} \text{trace}(\mathbf{T}(\mathbf{u}))) + \|\mathbf{G}\mathbf{d} - \mathbf{x}\|_2^2 \\ \text{s.t.} \quad & \begin{pmatrix} v & \mathbf{d}^H \\ \mathbf{d} & \mathbf{T}(\mathbf{u}) \end{pmatrix} \succeq 0. \end{aligned} \quad (17)$$

The algorithm flow for gridless DoA estimation on NLAs by ANM (denoted as NLANM) is organized in Alg. 2.

---

#### Algorithm 2: NLANM

---

**Input:**  $\mathbf{x}$ ,  $\tau$ ,  $K$ ,  $\mathbf{r}$ .

**Output:**  $\{(\hat{c}_k, \hat{\theta}_k)\}$ .

1. Calculate the sampling matrix  $\mathbf{G}$  based on Eq. (14) and Eq. (15);
2. Solve the SDP problem of Eq. (17);
3. Performed eigenvalue decomposition on  $\mathbf{T}(\mathbf{u})$ ;
4. Determine the noise subspace  $\mathbf{U}_N$  based on the number of targets  $K$ ;
5. Define  $\mathbf{p}(z) = [z^{-I} \ \dots \ 1 \ \dots \ z^I]^T$ ,  $f(z) = \mathbf{p}^H(z) \mathbf{U}_N \mathbf{U}_N^H \mathbf{p}(z)$  and find the roots of the polynomial  $f(z)$ ;
6. Find the  $K$  roots  $\{z_k\}$  closest to the unit circle;
7. Calculate  $\{\hat{\theta}_k\}$  based on

$$\hat{\theta}_k = \text{abs}(\text{angle}(z_k)),$$

where  $\text{abs}(\text{angle}(z_k))$  returns the absolute value of  $\text{angle}(z_k)$ ;

8. The reflectivity  $\{\hat{c}_k\}$  can be calculated by the least squares method.
- 

2) *Acceleration method*: Based on the manifold separation technique, we successfully extended the ANM algorithm – which can only be applied to ULAs – to NLAs, and solved the problem by SDP. However, the feasibility of SDP is highly limited by the problem scale. In fact, the computational complexity of the SDP is  $\mathcal{O}(N^{3.5})$ , where  $N$  is the number of array elements [39]. This is a huge computational load. When  $N$  is larger than 32, it is usually inapplicable in practice. However, for the extension of the ANM algorithm to NLAs, we construct a new virtual array from the sampling matrix. The

virtual array consists of  $N_v = 2I + 1$  array elements, where  $I > \frac{2\pi}{\lambda} D$ . Thus, the complexity of SDP in Alg. 2 should be  $\mathcal{O}(N_v^{3.5})$ , which is usually unacceptable.

In this paper, inspired by [31], we solve the above SDP problem (17) by APG and iterative shrinkage thresholding to reduce the solution complexity to  $\mathcal{O}(N_v^2)$ . APG can handle a variety of optimization problems with different constraints, including convex optimization problems with sparsity and low-rank constraints, by iteratively performing the three steps of smoothing, gradient descent, and approximate mapping. Considering the Vandermonde structure of  $\mathbf{v}(\theta)$  and the sparsity of  $\theta$ , we add a threshold shrinkage step after gradient descent to guarantee the low-rank property of the Toeplitz matrix  $\mathbf{T}(\mathbf{u})$ . The flow is shown in Alg. 3.

---

**Algorithm 3: APG**


---

**Input:**  $\mathbf{x}$ ,  $\mathbf{G}$ ,  $\epsilon$ , maxiter.

**Output:**  $\mathbf{T}(\mathbf{u})$ .

**Initialize:**

- $i = 1$ ,  $t_0 = 1$ ,  $\mathbf{d}^0 = \mathbf{G}^H \mathbf{x}$ ;
- $\mathbf{T}_0 = \mathcal{T}(\mathbf{d}_0 \mathbf{d}_0^H)$ , where  $\mathcal{T}(\mathbf{d}_0 \mathbf{d}_0^H)$  returns a Toeplitz matrix by averaging all elements along each diagonal direction of  $\mathbf{d}_0 \mathbf{d}_0^H$ ;
- $v_0 = \text{trace}(\mathbf{T}_0) / N_v$ ,
- $\mathbf{f}_1 = \mathbf{f}_0 = (\mathbf{d}_0, v_0, \mathbf{T}_0)$ .

**repeat**

1. Set  $\bar{\mathbf{f}}_i = \mathbf{f}_i + \frac{t_{i-1}-1}{t_i}(\mathbf{f}_i - \mathbf{f}_{i-1}) = (\bar{\mathbf{d}}_i, \bar{v}_i, \bar{\mathbf{T}}_i)$ , where  $t_i = \frac{1 + \sqrt{4t_{i-1}^2 + 1}}{2}$ ;
  2. Calculate  $\mathbf{d}_g = \bar{\mathbf{d}}_i - \delta \mathbf{G}^H (\mathbf{G} \bar{\mathbf{d}}_i - \mathbf{x})$ ,  $v_g = \bar{v}_i$  and  $\mathbf{T}_g = \bar{\mathbf{T}}_i$ , where  $\delta$  is an appropriate small stepsize;
  3. Decompose  $\mathbf{T}_g$  into  $\mathbf{T}_g = \mathbf{V} \mathbf{\Lambda} \mathbf{V}^H$ ;
  4. Shrink  $\mathbf{\Lambda}$  to  $\tilde{\mathbf{\Lambda}}$  and set  $\tilde{\mathbf{T}}_g = \mathbf{V} \tilde{\mathbf{\Lambda}} \mathbf{V}^H$ ;
  5. Set  $\mathbf{Z} = [\text{trace}(\tilde{\mathbf{\Lambda}}) \mathbf{d}_g^H; \mathbf{d}_g \tilde{\mathbf{T}}_g]$  and decompose  $(\mathbf{\Sigma}, \mathbf{U}) = \text{eigs}(\mathbf{Z}, \text{rank}(\tilde{\mathbf{\Lambda}}) + 1)$ ;
  6. Set  $\tilde{\mathbf{Z}} = \mathbf{U} \mathbf{\Sigma} \mathbf{U}^H$ ;
  7. Update  $\theta_{i+1} = (\mathbf{d}_{i+1}, v_{i+1}, \mathbf{T}_{i+1})$ , where  $\mathbf{d}_{i+1} = \tilde{\mathbf{Z}}_{2:\text{end}, 1}$ ,  $v_{i+1} = \tilde{\mathbf{Z}}_{1, 1}$ , and  $\mathbf{T}_{i+1} = \tilde{\mathbf{Z}}_{2:\text{end}, 2:\text{end}}$ ;
  8.  $i = i + 1$ ;
- until**  $i > \text{maxiter}$  or  $\|\mathbf{T}_{i+1} - \mathbf{T}_i\|_F \leq \epsilon$   
 $\mathbf{T}(\mathbf{u}) = \mathbf{T}_{i+1}$ .
- 

The proposed method is named as the FNLANM algorithm (from the acoustic fast NLANM), which is a fast implementation of the NLANM algorithm. This proposed method achieves accelerated gridless DoA estimation for arbitrary linear arrays. The detailed algorithm flow is given in Alg. 4, and the computational complexity is given in Tab. I.

#### IV. SIMULATION EXPERIMENTS

##### A. Performance metrics

1) *Accuracy:* We measure the accuracy of DoA estimation in terms of the root mean square error (RMSE) between the DoA estimated result  $\hat{\theta}$  and the ground truth  $\theta_0$ . RMSE is defined as follows

$$\text{RMSE} = \sqrt{\frac{\sum_{i=1}^{MC} \|\hat{\theta}_i - \theta_0\|_2^2}{MC \times K}}, \quad (18)$$

---

**Algorithm 4: FNLANM**


---

**Input:**  $\mathbf{x}$ ,  $\tau$ ,  $K$ ,  $\mathbf{r}$ ,  $\epsilon$ , maxiter.

**Output:**  $\{(\hat{c}_k, \hat{\theta}_k)\}$ .

1. Calculate the sampling matrix  $\mathbf{G}$  based on Eq. (15);
2.  $\mathbf{T}(\mathbf{u}) = \text{APG}(\mathbf{x}, \mathbf{G}, \epsilon, \text{maxiter})$ ;
3. Performed eigenvalue decomposition on  $\mathbf{T}(\mathbf{u})$ ;
4. Determine the noise subspace  $\mathbf{U}_N$  based on the number of targets  $K$ ;
5. Define  $\mathbf{p}(z) = [z^{-I} \ \cdots \ 1 \ \cdots \ z^I]^T$ ,  $f(z) = \mathbf{p}^H(z) \mathbf{U}_N \mathbf{U}_N^H \mathbf{p}(z)$  and find the roots of the polynomial  $f(z)$ ;
6. Find the  $K$  roots  $\{z_k\}$  closest to the unit circle;
7. Calculate  $\{\hat{\theta}_k\}$  based on

$$\hat{\theta}_k = \text{abs}(\text{angle}(z_k)),$$

where  $\text{abs}(\text{angle}(z_k))$  returns the absolute value of  $\text{angle}(z_k)$ ;

8. The reflectivity  $\{\hat{c}_k\}$  can be calculated by the least squares method.
- 

TABLE I: Computational complexity.

Algorithm	ANM	NLANM	FNLANM
Computational complexity	$\mathcal{O}(N^{3.5})$	$\mathcal{O}(N_v^{3.5})$	$\mathcal{O}(N_v^2)$

where  $MC$  is the number of Monte Carlo experiments and  $K$  is the number of targets.

2) *Robustness:* We measure the robustness of DoA estimation in terms of the success rate, which is defined as follows

$$\text{SR} = \frac{mc_t}{MC}, \quad (19)$$

where  $mc_t$  is the total amount of experiments that satisfy  $\max |\hat{\theta} - \theta_0| < \gamma$  and  $\gamma$  is a constant small enough.

##### B. Non-uniform linear array

In this subsection, we aim to prove the necessity of extending ANM to NLAs by setting arrays with different location deviations (LD). We compare the NLA and ULA with the same aperture  $D$  and the number of elements  $N$ , and define the location deviation as follows:

$$\text{LD} = \sqrt{\frac{\|\mathbf{r} - \mathbf{r}_{ula}\|_2^2}{N}} / d, \quad (20)$$

where

- $\mathbf{r} = [0 \ r_1 \ \cdots \ r_{N-1}]^T$  is the position of each array element of the NLA;
- $\mathbf{r}_{ula} = [0 \ d \ \cdots \ (N-1)d]^T$  is the position of each array element of the ULA.

The influence of location deviation on the estimation accuracy of the three ANM-based algorithms is discussed through multiple Monte Carlo experiments. In this experiment, we increase location deviation progressively and other simulation parameters are shown in Tab. II.

At each location deviation, 1000 different arrays are randomly generated and DoA estimation is performed by ANM,

TABLE II: Simulation parameters.

Parameters	Symbols	Values
Frequency	$f$	77.5 GHz
Number of array elements	$N$	16
Aperture	$D$	29.0 mm
Signal-to-noise ratio	SNR	30 dB

NLANM and FNLANM algorithms. The RMSEs of the three algorithms are shown in Fig. 2. It can be seen that the RMSE of ANM increases rapidly with the increase of LD. When LD reaches 0.3, the RMSE of ANM approaches  $10^\circ$ , which means that in almost all tested arrays of  $LD = 0.3$ , the difference between the DoA estimated result and the ground truth is large. Such extremely unreliable estimates cannot be applied in practice. However, the RMSEs of NLANM and FNLANM are not affected by the location deviation. The complexities and the average computation times of DoA estimation algorithms are given in Tab. III. For computation, Intel CPU i5-8265U (1.60 GHz) and 8 GB RAM are used. It is worth mentioning that FNLANM greatly reduces the average runtime while maintaining almost the same DoA estimation accuracy as NLANM.

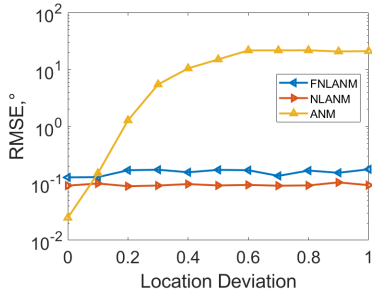


Fig. 2: Estimation accuracy comparison of ANM, NLANM and FNLANM versus location deviation.

TABLE III: Average runtime.

Algorithm	ANM	NLANM	FNLANM
Average runtime,s	1.7	34.3	6.0

This statistical experiment demonstrates the necessity of extending the existing frame of the ANM algorithm to NLANM and accelerating the algorithm.

### C. Off-grid effect

All the following simulation experiments are based on NLAs. The simulation parameters are shown in the Tab. IV, where the super-resolution factor is a constant relative to the grid interval of grid-based CS algorithms. The theoretical resolution of the system  $\rho$  and the grid interval  $\rho_s$  can be calculated according to Eq. (21) and Eq. (22) [40].

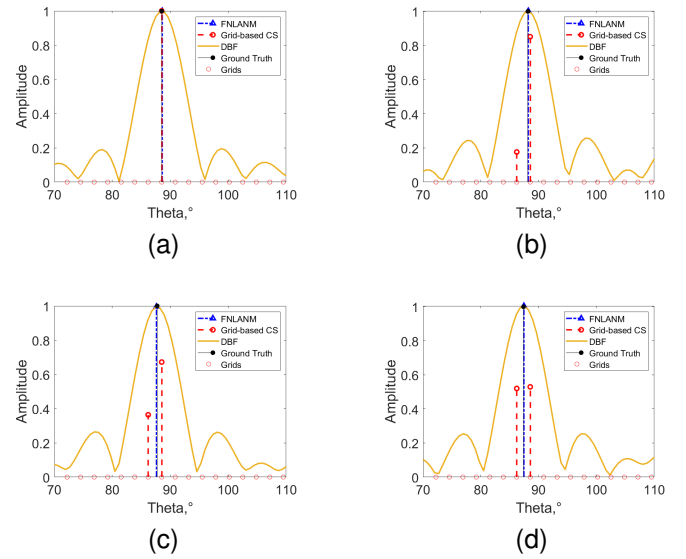
$$\rho = 1.22 \frac{\lambda}{D} \quad (21)$$

TABLE IV: Simulation parameters.

Parameters	Symbols	Values
Frequency	$f$	77.5 GHz
Number of array elements	$N$	16
Aperture	$D$	29.0 mm
Location deviation	$LD$	0.3
Signal-to-noise ratio	SNR	20 dB
Super-resolution factor	$\eta$	4

$$\rho_s = \frac{\rho}{\eta} \quad (22)$$

The DoA estimation results of DBF, grid-based CS and the proposed algorithm FNLANM are compared by setting a single target at different positions. By comparing the results in Fig. 3, we can see that: for the grid-based CS algorithm, when the target is off the grid, the energy of the real target will leak to the nearby grid, resulting in the difference between the predicted sparsity and the real sparsity, causing false alarms and missed alarms. This effect becomes more severe as the off-grid error becomes larger. However, DBF and FNLANM are completely unaffected by the off-grid effect. With this simple example, we show the impact of the off-grid effect on the DoA estimation performance of grid-based CS algorithms, which in turn illustrates the necessity of research on gridless DoA estimation methods.

Fig. 3: Comparison of estimation results of DBF, grid-based CS and FNLANM. The off-grid error of the single target is (a) 0, (b)  $\rho_s/6$ , (c)  $\rho_s/3$ , (d)  $\rho_s/2$ .

Next, we investigate the estimation performance of three algorithms for an off-grid target through Monte Carlo experiments. The RMSEs of the three algorithms are compared with the Cramér-Rao lower bound (CRLB). We set  $\gamma = \rho_s/2$  and calculate the success rates of the three algorithms according to Eq. (19). As seen in Fig. 4, the estimation performance of all three algorithms becomes better with increasing SNR with the

same trend. As the SNR rises to 8 dB, the RMSE of grid-based CS decreases rapidly and then plateaus, eventually stabilizing at a constant associated with the off-grid error of the target. However, the RMSEs of ANM and DBF are almost the same when the SNR is less than 10 dB, and are much better than the grid-based CS algorithm for all tested SNRs. When the SNR is large than 20 dB, the RMSE decline of the DBF algorithm becomes flat and almost no longer decreases with increasing SNR, while the ANM is always approaching the CRLB.

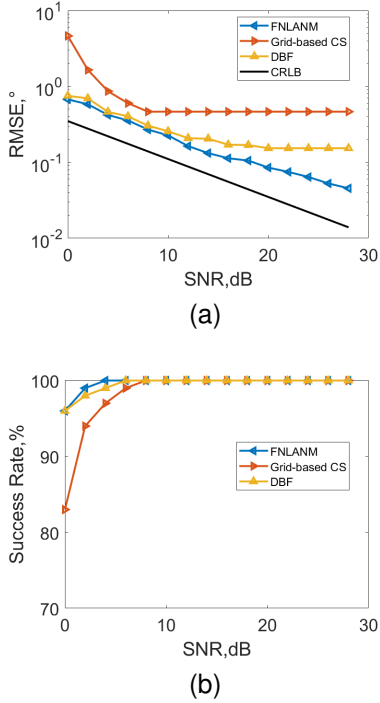


Fig. 4: Estimation performance of DBF, grid-based CS and FNLANM for an off-grid target versus the SNR. (a) RMSE. (b) SR for  $\gamma = \rho_s/2$ .

From this experiment, we can conclude that for the DoA estimation of an off-grid target, the accuracy and robustness of the FNLANM algorithm outperform the grid-based CS algorithm.

#### D. Number of array elements

In this part of the experiment, we investigate the effect of the number of array elements  $N$  on the DoA estimation performance for a certain array aperture  $D$ . To demonstrate more clearly, a variable is defined as

$$\alpha = \frac{N}{N_{ula}}, \quad (23)$$

where  $N_{ula}$  is the number of array elements of a standard ULA satisfying  $D = \frac{(N_{ula}-1)\lambda}{2}$ .

We simulate  $N_{ula} = 16$ ,  $D = 29.0$  mm,  $LD = 0.3$ , and  $\alpha = \{0.5, 1.0, 1.5, 2.0\}$  respectively, and evaluate the estimation performance as a function of the SNR. The experimental results of DoA estimation by FNLANM for different  $\alpha$  are shown in Fig. 5, and the average runtimes are shown in Tab. V. As seen in the results, the estimation performance

all becomes better with increasing SNR with the same trend for different  $\alpha$ . When  $\alpha = 0.5$ , a SNR greater than 14 dB is required to achieve a valid and stable DoA estimate. When  $\alpha$  increases from 0.5 to 1.0, both RMSE and SR gain significant improvements, especially at SNR below 14 dB. However, when  $\alpha$  continues to increase, the enhancement of both evaluation metrics is no longer significant. It is interesting to mention that the number of array elements  $N$  has almost no effect on the average runtime with a constant array aperture  $D$ .

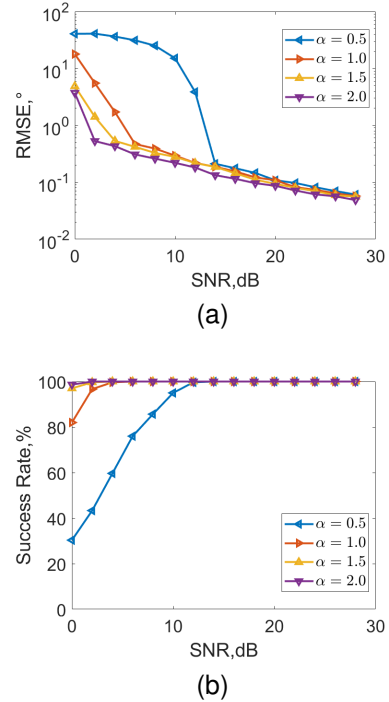


Fig. 5: Estimation performance of FNLANM for different  $\alpha$  versus the SNR. (a) RMSE. (b) SR for  $\gamma = \rho/4$ .

TABLE V: Average runtime.

$\alpha$	0.5	1.0	1.5	2.0
Average runtime,s	5.9	6.0	6.0	6.1

This experiment illustrates that for a certain array aperture, it is not necessary for FNLANM to pursue a dense array element arrangement to achieve a better DoA estimation performance, which helps to reduce the amount of data collection.

#### E. Array aperture

In this part of the experiments, we keep  $\alpha$  constant and investigate the effect of array aperture  $D$  on the DoA estimation performance.

We simulate  $\alpha = 1.0$ ,  $LD = 0.3$  and  $D = \{2, 4, 6, 8, 10\}\lambda$  respectively, and evaluate the estimation performance as a function of the SNR. The experimental results of DoA estimation by FNLANM for different  $D$  are shown in Fig. 6. From the results, it can be seen that the different  $D$  have the

same tendency to become better in estimation performance as the SNR increases. When  $D = 2\lambda$ , a SNR greater than 10 dB is required to obtain a valid and stable DoA estimate for a single target. When  $D$  is increased from  $2\lambda$  to  $4\lambda$ , a significant improvement of RMSE is obtained at all tested SNRs. However, as  $D$  continues to increase, the RMSE still improves, but the improvement becomes progressively smaller. The effect of  $D$  on SR is mainly reflected when the SNR is below 10 dB. A larger array aperture can achieve a higher success rate of DoA estimation at low SNR. However, it can be seen from Fig. 6c that although the proposed method FNLANM is already an improved algorithm after accelerating the NLANM algorithm by APG, its average runtime still rises rapidly when the array aperture  $D$  increases.

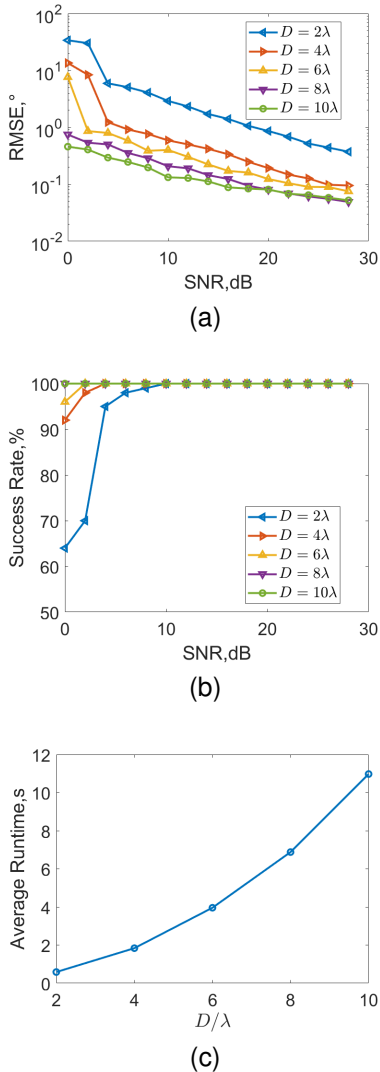


Fig. 6: Estimation performance of FNLANM for different  $D$ . (a) RMSE versus the SNR. (b) SR versus the SNR for  $\gamma = \rho/4$  (c) Average runtime.

This experiment illustrates that it is not necessary for FNLANM to pursue massive arrays to obtain better DoA estimation performance, which helps to reduce the hardware requirements.

### F. Angular super-resolution

Theoretically, when the distance between two targets is larger than the theoretical resolution  $\rho$ , DBF, grid-based CS and ANM all can separate the two targets; when the distance between two targets is smaller than the theoretical resolution  $\rho$ , DBF cannot separate them, while both grid-based CS and ANM have super-resolution capability to separate the two targets. We simulate  $K = 2$  targets with  $\theta_1 \in [0, \pi]$  and  $\theta_2 = \theta_1 - \Delta\theta$  in this experiment and evaluate the estimation performance as a function of  $\Delta\theta$ .

Setting  $\Delta\theta = \{\rho, \rho_s\}$  and setting  $\theta_1$  off-grid and on-grid respectively, the experimental results are shown in Fig. 7. By comparing Fig. 7a and Fig. 7b, we can see that when the angular separation between two targets is large enough, whether the targets are off-grid or not only affects the reconstruction performance of the grid-based CS algorithm, while both DBF and FNLANM can accurately locate two targets. By comparing Fig. 7a and Fig. 7c, we can see that when the angular separation of two on-grid targets is less than the theoretical resolution  $\rho$ , both the grid-based CS algorithm and FNLANM exhibit super-resolution capability to separate the targets. Comparing Fig. 7c and Fig. 7d, we can see that the super-resolution capability of grid-based CS is severely affected by the off-grid effect, and only FNLANM among the three algorithms can accurately locate two targets when the angular separation between two off-grid targets is less than the theoretical resolution.

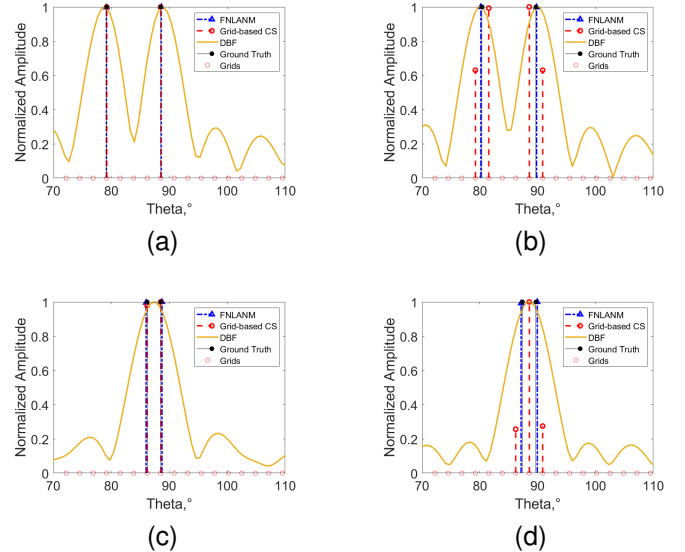


Fig. 7: Comparison of reconstruction results by DBF, grid-based CS and FNLANM. (a) On-grid targets with  $\Delta\theta = \rho$ . (b) Off-grid targets with  $\Delta\theta = \rho$ . (c) On-grid targets with  $\Delta\theta = \rho_s$ . (d) Off-grid targets with  $\Delta\theta = \rho_s$ .

With the simulation parameters as shown in Tab. IV, setting  $\theta_1 = 90^\circ$  and gradually increasing  $\Delta\theta$  from 0 to  $2\rho$ , the DoA estimation results are shown in Fig. 8. The results show that with the theoretical resolution  $\rho = 9.32^\circ$ , FNLANM can separate the targets that are  $2.45^\circ$  apart, which demonstrates a good super-resolution capability. However, the super-

resolution capability of the grid-based CS algorithm is severely deteriorated because of the off-grid effect.

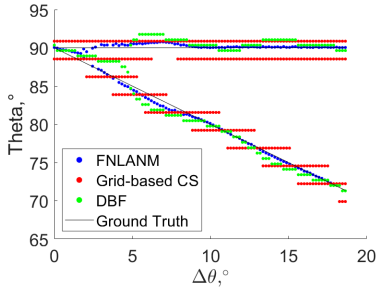


Fig. 8: Comparison of estimation results by DBF, grid-based CS and FNLANM versus angular separation for  $N = 16$ ,  $D = 29.0$  mm,  $\text{SNR} = 20$  dB.

To better investigate the super-resolution ability of FNLANM, we examine the variation of RMSE and SR with  $\Delta\theta \in (0, \rho)$  under different SNRs by statistical experiments, and the results are shown in Fig. 9. The experimental results conform to the expectation that the estimation performance of FNLANM becomes better as the SNR increases. When the  $\text{SNR} = 0$  dB, FNLANM can achieve almost unreliable DoA estimation. When the SNR rises to 10 dB, FNLANM can stably separate targets with an interval slightly smaller than  $\rho$ . As the SNR rises to 20 dB, FNLANM can separate targets spaced approximately  $\rho/3$  apart. As the SNR continues to rise, the minimum  $\Delta\theta$  that can be separated hardly changes anymore.

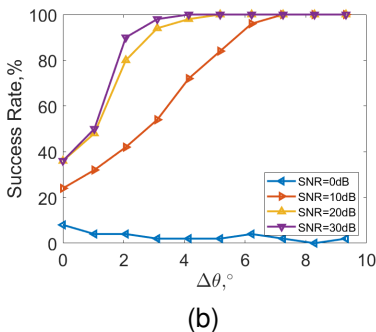
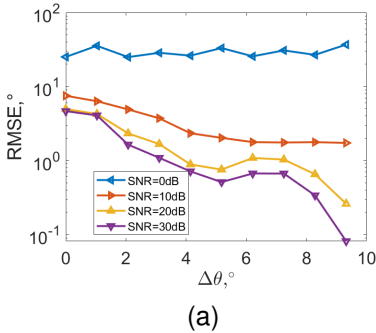


Fig. 9: Estimation performance of FNLANM for different SNRs versus angular separation. (a) RMSE. (b) SR for  $\gamma = \rho/4$ .

To summarize, FNLANM has super-resolution capability with a resolution of  $\rho/3$  at a sufficiently high SNR. The experiments in this subsection illustrate the superiority of FNLANM in terms of super-resolution.

### G. Automotive scenario

Through the above simulation experiments, we prove the advantages of the proposed algorithm FNLANM in DoA estimation. In this section, we simulate an actual driving scenario to visualize it. For this purpose, corner reflectors are used to obtain the point target radar response. As shown in Fig. 10a, the radar sensor remains stationary and the two corner reflectors are 3 m apart and moving side-by-side in the direction away from the radar sensor. Fig. 10b shows the directions of arrival of the two corner reflectors, as the range increases from 10 m to 50 m. According to the setting of the simulation scene, the angle of the two corner reflectors is continuously changed with the range, and the minimum angular separation of the two corner reflectors is  $3.4^\circ$ .

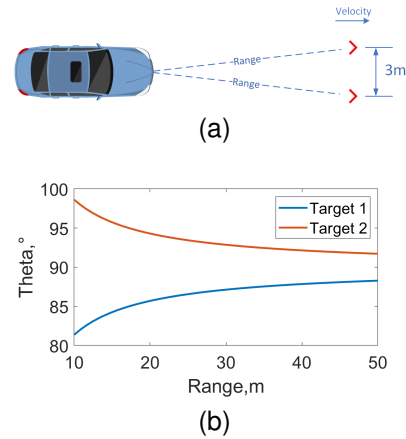


Fig. 10: (a) Simulation scenes. (b) Directions of arrival.

The simulation parameters are the same as Tab. IV and the results of DBF, grid-based CS and FNLANM for the simulated scenario are shown in Fig. 11. We use two black lines to indicate the ground truth of the two corner reflectors.

Fig. 11a shows that DBF is less affected by the off-grid effect, but the resolution is poor. When the angular separation of two corner reflectors is less than the theoretical resolution  $\rho$ , DBF cannot separate them. As can be seen from Fig. 11b, the results of the grid-based CS method are heavily affected by the off-grid effect. More spurious targets appear and the estimated reflectivities of the corner counters have large errors. It is evident from Fig. 11c that FNLANM always locates two corner reflectors precisely, with no off-grid effect at all, and can reconstruct both corner reflectors accurately even when the angular separation between two corner reflectors is significantly less than the theoretical resolution.

This part of the experiment visualizes the off-grid effect and the advantages of FNLANM by continuously varying the DoA of two corner reflectors.

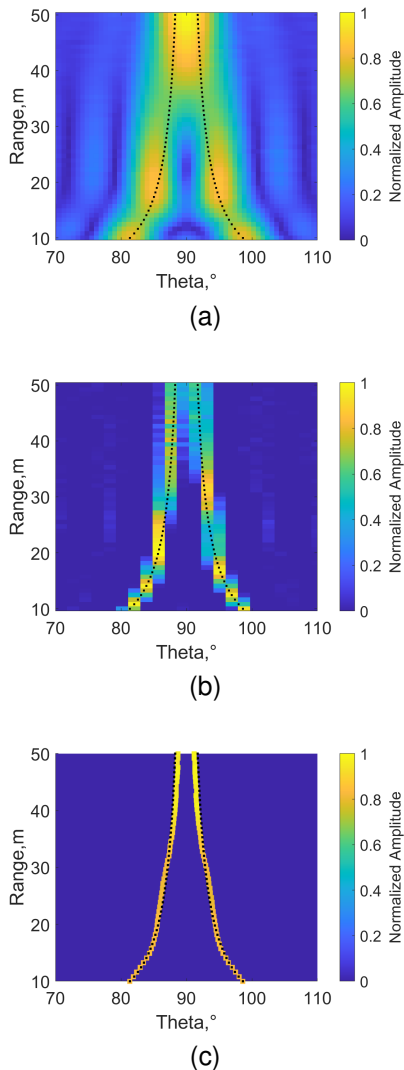


Fig. 11: DoA results of scenario simulation. (a) DBF. (b) Grid-based CS. (c) FNLANM.

## V. MEASUREMENT EXPERIMENTS

### A. Measurement setup

We use two sets of measured data to demonstrate that the FNLANM algorithm proposed in this paper can be directly applied to current radar systems. The two radars used in the measurement experiments are both designed by Beijing Autoroad Tech. Co. Ltd, and the radar parameters are shown in the following Tab. VI. Radar 1 is a 77 GHz short range radar with 600 MHz bandwidth, 3 transmitting and 4 receiving antenna. Radar 2 is a 77 GHz 4D automotive radar with 2 GHz bandwidth, 4 transmitting and 8 receiving antenna.

As shown in Fig. 12, the data were collected in a park with 1 or 2 corner reflectors as the main targets. The radar calibration matrices were measured under darkroom turntable conditions with an interval of  $0.5^\circ$ . By analyzing the calibration matrices, the precise position of each array element and the channel phase can be obtained, and an accurate observation matrix can be constructed. The observation matrix used in the experiment in this section is obtained by the above method. Moreover,

TABLE VI: Radar parameters.

Radar 1		
Parameters	Symbols	Values
Frequency,GHz	$f$	77.5
Bandwidth,GHz	$B$	0.6
Transmitting antenna,mm	Tx	0,5,7,11,4
Receiving antenna,mm	Rx	0,3,8,7,6,11,4
Theoretical resolution, $^\circ$	$\rho$	11.9
Radar 2		
Parameters	Symbols	Values
Frequency,GHz	$f$	77.9
Bandwidth,GHz	$B$	2
Transmitting antenna,mm	Tx	0,8,38,68
Receiving antenna,mm	Rx	0,28,32,52,64,78,104,118
Theoretical resolution, $^\circ$	$\rho$	1.5

there may be bias in the experimental field measurements or bias in the calibration process. The maximum likelihood (ML) estimate should be considered as the ground truth when validating DoA estimation methods, considering that ML is the optimal estimate under the Gaussian noise model [41].



Fig. 12: Realistic test scenario.

As we can see from the radar parameters, automotive radars are usually based on MIMO radars, and virtual arrays are hardly ULAs, so it makes sense to study DoA estimation algorithms that are applicable to arbitrary array forms. Also, in the real world, targets can be located anywhere in space, so those located on the grids are very few, and most of them are off the grids. Therefore it is meaningful to study gridless sparse DoA estimation applicable to arbitrary arrays.

### B. Measurement results

A total of six experiments are conducted on radar 1, four of which are single corner reflector experiments and two of which are double corner reflectors experiments. The DoA estimation results for the data acquired by radar 1 are shown in Fig. 13. From the DoA estimation results of the single corner reflector, it can be seen that both DBF and FNLANM can estimate the DoA accurately, while the performance of the grid-based CS method is affected by the off-grid error of the target. Fig. 13c shows the results when the corner reflectors in Fig. 13a and Fig. 13b are present simultaneously, and the angular separation of them is  $\Delta\theta = 12.7^\circ$ , which is greater than the theoretical resolution. Experimental results show that only the grid-based CS method suffers from the off-grid effect, while both DBF and FNLANM are able to separate and accurately locate the two targets with  $\Delta\theta > \rho$ . Just as Fig. 13c, the targets of Fig. 13f are a combination of Fig. 13d

and Fig. 13e, with the two corner reflectors separated by  $\Delta\theta = 7.7^\circ$ . The experimental results show that FNLANM still exhibits excellent DoA estimation performance when  $\Delta\theta < \rho$ , which is much better than that of DBF and grid-based CS.

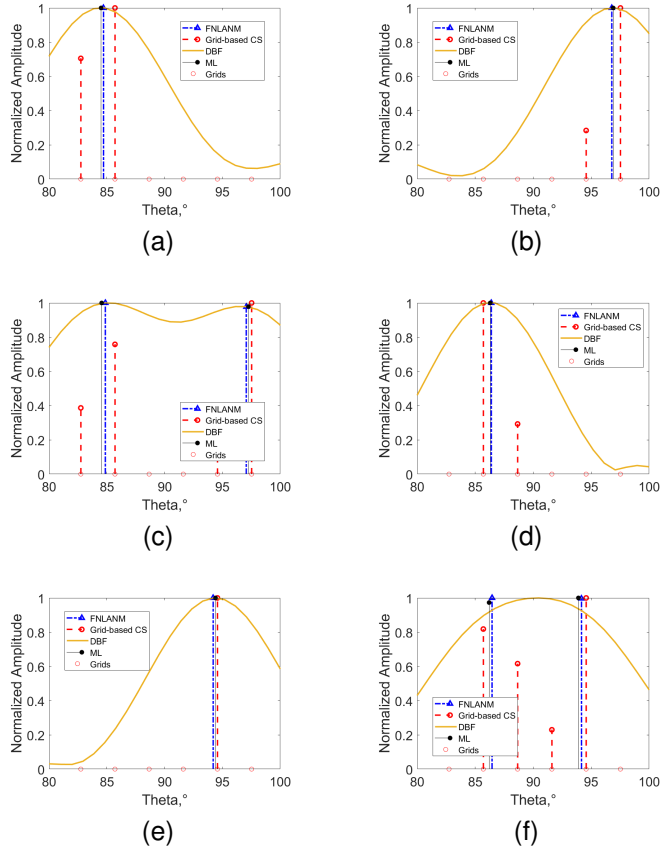


Fig. 13: DoA estimation results of radar 1.

The theoretical resolution of radar 2 is better than that of radar 1. All the experiments conducted on radar 2 are double corner reflectors experiments, which are mainly used to investigate the resolution capability of the proposed DoA estimation algorithm. The DoA estimation results for the data acquired by radar 2 are shown in Fig. 14. During the four experiments, the angular separation of the two corner reflectors gradually decreases, and FNLANM is always able to accurately locate their directions and separate them, regardless of whether the targets are off-grid or not.

The experimental results of measured data acquired by automotive MIMO radars from Beijing Autoroad Tech Co., Ltd are compatible with the analysis of theory and simulation experiments. When the target is not precisely located in the grids, there is a high possibility that the energy of the off-grid target will leak to several grids near the ground truth, leading to inaccurate DoA estimates and even false targets of the grid-based CS method. The measurement experiments have verified that FNLANM fundamentally avoids the grid mismatch problem and has super-resolution capability.

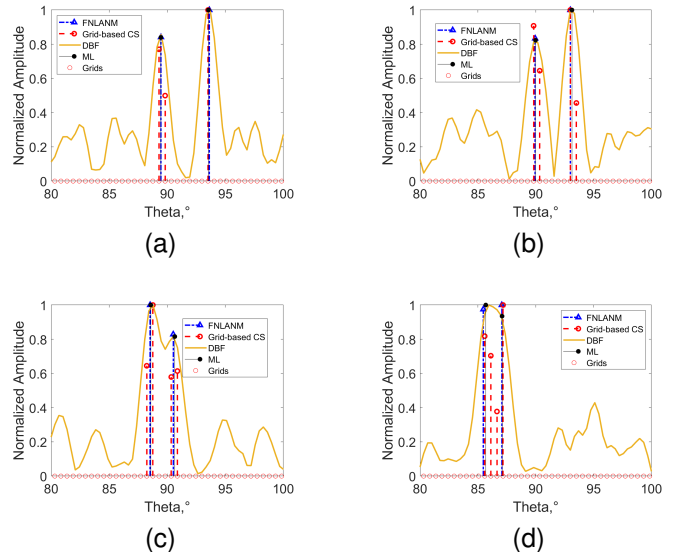


Fig. 14: DoA estimation results of radar 2. (a)  $\Delta\theta = 4.2^\circ$ , (b)  $\Delta\theta = 3.1^\circ$ , (c)  $\Delta\theta = 2.1^\circ$ , (d)  $\Delta\theta = 1.4^\circ$ .

## VI. CONCLUSION

In this paper, the gridless DoA estimation problem for NLAs is studied. The author proposes a fast gridless DoA estimation algorithm for NLAs based on ANM, which combines the array manifold separation technique and a priori knowledge based acceleration technique to reduce the computational complexity by 1.5 orders. The simulation results indicate that the proposed FNLANM algorithm successfully extends ANM algorithm to arbitrary linear arrays with acceptable computational complexity. The proposed algorithm is also validated on the automotive MIMO radars designed by Beijing Autoroad Tech Co., Ltd.

Future work will focus on the super-resolution ability and further reduction of the computational complexity, as well as the noise robustness.

## REFERENCES

- [1] J. Capon, "High-resolution frequency-wavenumber spectrum analysis," *Proceedings of the IEEE*, vol. 57, no. 8, pp. 1408–1418, 1969.
- [2] R. Schmidt, "Multiple emitter location and signal parameter estimation," *IEEE Transactions on Antennas and Propagation*, vol. 34, no. 3, pp. 276–280, 1986.
- [3] M. Pesavento, A. B. Gershman, and M. Haardt, "Unitary root-MUSIC with a real-valued eigendecomposition: A theoretical and experimental performance study," *IEEE transactions on signal processing*, vol. 48, no. 5, pp. 1306–1314, 2000.
- [4] R. Roy and T. Kailath, "ESPRIT-estimation of signal parameters via rotational invariance techniques," *IEEE Transactions on Acoustics, Speech, and Signal Processing*, vol. 37, no. 7, pp. 984–995, 1989.
- [5] M. Haardt and J. A. Nosssek, "Unitary ESPRIT: How to obtain increased estimation accuracy with a reduced computational burden," *IEEE transactions on signal processing*, vol. 43, no. 5, pp. 1232–1242, 1995.
- [6] A. Hu, T. Lv, H. Gao, Z. Zhang, and S. Yang, "An ESPRIT-based approach for 2-D localization of incoherently distributed sources in massive MIMO systems," *IEEE Journal of Selected Topics in Signal Processing*, vol. 8, no. 5, pp. 996–1011, 2014.
- [7] W. Li, W. Liao, and A. Fannjiang, "Super-resolution limit of the ESPRIT algorithm," *IEEE transactions on information theory*, vol. 66, no. 7, pp. 4593–4608, 2020.
- [8] D. L. Donoho, "Compressed sensing," *IEEE Transactions on Information Theory*, vol. 52, no. 4, pp. 1289–1306, 2006.

- [9] R. Baraniuk, "Compressive sensing [lecture notes]," *IEEE Signal Processing Magazine*, vol. 24, no. 4, pp. 118–121, 2007.
- [10] E. J. Candes and M. B. Wakin, "An introduction to compressive sampling," *IEEE Signal Processing Magazine*, vol. 25, no. 2, pp. 21–30, 2008.
- [11] D. Malioutov, M. Cetin, and A. S. Willsky, "A sparse signal reconstruction perspective for source localization with sensor arrays," *IEEE Transactions on Signal Processing*, vol. 53, no. 8, pp. 3010–3022, 2005.
- [12] J. Yin and T. Chen, "Direction-of-arrival estimation using a sparse representation of array covariance vectors," *IEEE Transactions on Signal Processing*, vol. 59, no. 9, pp. 4489–4493, 2011.
- [13] Y. Chi, L. L. Scharf, A. Pezeshki, and A. R. Calderbank, "Sensitivity to basis mismatch in compressed sensing," *IEEE Transactions on Signal Processing*, vol. 59, no. 5, pp. 2182–2195, 2011.
- [14] X. Wu, W.-P. Zhu, J. Yan, and Z. Zhang, "Two sparse-based methods for off-grid direction-of-arrival estimation," *Signal Processing*, vol. 142, pp. 87–95, 2018.
- [15] E. Candès, "The restricted isometry property and its implications for compressed sensing," *Comptes Rendus Mathématique*, vol. 346, no. 9–10, pp. 589–592, 2008.
- [16] H. Zhu, G. Leus, and G. B. Giannakis, "Sparsity-cognizant total least-squares for perturbed compressive sampling," *IEEE Transactions on Signal Processing*, vol. 59, no. 5, pp. 2002–2016, 2011.
- [17] Z. Yang, L. Xie, and C. Zhang, "Off-grid direction of arrival estimation using sparse Bayesian inference," *IEEE Transactions on Signal Processing*, vol. 61, no. 1, pp. 38–43, 2013.
- [18] M. Carlin, P. Rocca, G. Oliveri, F. Viani, and A. Massa, "Directions-of-arrival estimation through Bayesian compressive sensing strategies," *IEEE Transactions on Antennas and Propagation*, vol. 61, no. 7, pp. 3828–3838, 2013.
- [19] L. Zhao, X. Li, L. Wang, and G. Bi, "Computationally efficient wide-band DOA estimation methods based on sparse Bayesian framework," *IEEE Transactions on Vehicular Technology*, vol. 66, no. 12, pp. 11 108–11 121, 2017.
- [20] P. Chen, Z. Cao, Z. Chen, and X. Wang, "Off-grid DOA estimation using sparse Bayesian learning in MIMO radar with unknown mutual coupling," *IEEE Transactions on Signal Processing*, vol. 67, no. 1, pp. 208–220, 2019.
- [21] G. Tang, B. N. Bhaskar, P. Shah, and B. Recht, "Compressed sensing off the grid," *IEEE Transactions on Information Theory*, vol. 59, no. 11, pp. 7465–7490, 2013.
- [22] X. Wu, W.-P. Zhu, and J. Yan, "A Toeplitz covariance matrix reconstruction approach for direction-of-arrival estimation," *IEEE Transactions on Vehicular Technology*, vol. 66, no. 9, pp. 8223–8237, 2017.
- [23] C. Zhou, Y. Gu, X. Fan, Z. Shi, G. Mao, and Y. D. Zhang, "Direction-of-arrival estimation for coprime array via virtual array interpolation," *IEEE Transactions on Signal Processing*, vol. 66, no. 22, pp. 5956–5971, 2018.
- [24] T. Chen, L. Shi, and L. Guo, "Gridless direction of arrival estimation exploiting sparse linear array," *IEEE Signal Processing Letters*, vol. 27, pp. 1625–1629, 2020.
- [25] X. Wu and W.-P. Zhu, "Single far-field or near-field source localization with sparse or uniform cross array," *IEEE Transactions on Vehicular Technology*, vol. 69, no. 8, pp. 9135–9139, 2020.
- [26] F. Wang, Z. Tian, G. Leus, and J. Fang, "Direction of arrival estimation of wideband sources using sparse linear arrays," *IEEE Transactions on Signal Processing*, vol. 69, pp. 4444–4457, 2021.
- [27] Z. Yang and L. Xie, "On gridless sparse methods for line spectral estimation from complete and incomplete data," *IEEE Transactions on Signal Processing*, vol. 63, no. 12, pp. 3139–3153, 2015.
- [28] M. A. Doron and E. Doron, "Wavefield modeling and array processing .i. spatial sampling," *IEEE Transactions on Signal Processing*, vol. 42, no. 10, pp. 2549–2559, 1994.
- [29] —, "Wavefield modeling and array processing .ii. algorithms," *IEEE Transactions on Signal Processing*, vol. 42, no. 10, pp. 2560–2570, 1994.
- [30] —, "Wavefield modeling and array processing .iii. resolution capacity," *IEEE Transactions on Signal Processing*, vol. 42, no. 10, pp. 2571–2580, 1994.
- [31] Y. Wang and Z. Tian, "IVDST: A fast algorithm for atomic norm minimization in line spectral estimation," *IEEE Signal Processing Letters*, vol. 25, no. 11, pp. 1715–1719, 2018.
- [32] S. M. Patole, M. Torlak, D. Wang, and M. Ali, "Automotive radars: A review of signal processing techniques," *IEEE Signal Processing Magazine*, vol. 34, no. 2, pp. 22–35, 2017.
- [33] C. Zhou, Y. Gu, S. He, and Z. Shi, "A robust and efficient algorithm for coprime array adaptive beamforming," *IEEE Transactions on Vehicular Technology*, vol. 67, no. 2, pp. 1099–1112, 2018.
- [34] S. Lutz, K. Baur, and T. Walter, "77 GHz lens-based multistatic MIMO radar with colocated antennas for automotive applications," in *2012 IEEE/MTT-S International Microwave Symposium Digest*, 2012, pp. 1–3.
- [35] J. Shi, G. Hu, X. Zhang, and F. Sun, "Sparsity-based DOA estimation of coherent and uncorrelated targets with flexible MIMO radar," *IEEE Transactions on Vehicular Technology*, vol. 68, no. 6, pp. 5835–5848, 2019.
- [36] F. Belloni, A. Richter, and V. Koivunen, "DoA estimation via manifold separation for arbitrary array structures," *IEEE Transactions on Signal Processing*, vol. 55, no. 10, pp. 4800–4810, 2007.
- [37] M. A. Doran, E. Doron, and A. J. Weiss, "Coherent wide-band processing for arbitrary array geometry," *IEEE Transactions on Signal Processing*, vol. 41, no. 1, 1993.
- [38] A. B. Gershman, M. Rübamen, and M. Pesavento, "One-and two-dimensional direction-of-arrival estimation: An overview of search-free techniques," *Signal Processing*, vol. 90, no. 5, pp. 1338–1349, 2010.
- [39] I. Pólik and T. Terlaky, *Interior Point Methods for Nonlinear Optimization*. Berlin, Heidelberg: Springer Berlin Heidelberg, 2010, pp. 215–276.
- [40] J. Hasch, E. Topak, R. Schnabel, T. Zwick, R. Weigel, and C. Waldschmidt, "Millimeter-wave technology for automotive radar sensors in the 77 GHz frequency band," *IEEE Transactions on Microwave Theory and Techniques*, vol. 60, no. 3, pp. 845–860, 2012.
- [41] P. Stoica and K. C. Sharman, "Maximum likelihood methods for direction-of-arrival estimation," *IEEE Transactions on Acoustics, Speech, and Signal Processing*, vol. 38, no. 7, pp. 1132–1143, 1990.